JOURNAL OF GEOPHYSICAL RESEARCH, VOL. 113, D15S05, doi:10.1029/2007JD008856, 2008

Tropospheric Emission Spectrometer nadir spectral radiance comparisons

Mark W. Shephard,[1] Helen M. Worden,[2] Karen E. Cady-Pereira,[1] Michael Lampel,[3] Mingzhao Luo,[2] Kevin W. Bowman,[2] Edwin Sarkissian,[2] Reinhard Beer,[2] David M. Rider,[2] David C. Tobin,[4] Henry E. Revercomb,[4] Brendan M. Fisher,[2] Denis Tremblay,[3] Shepard A. Clough,[1] Gregory B. Osterman,[2] and Michael Gunson[2]

Received 19 April 2007; revised 15 October 2007; accepted 19 November 2007; published 22 April 2008.

[1] The fundamental measurement of the Tropospheric Emission Spectrometer (TES) on board the Aura spacecraft is upwelling infrared spectral radiances. Accurate TES retrievals of surface and atmospheric parameters such as trace gas amounts critically depend on well-calibrated radiance spectra. On-orbit TES nadir observations were evaluated using carefully selected, nearly coincident spectral radiance measurements from Atmospheric Infrared Sounder (AIRS) on Aqua and special scanning high-resolution interferometer sounder (SHIS) underflights. Modifications to the L1B calibration algorithms for TES version 2 data resulted in significant improvements for the TES-AIRS comparisons. The comparison of TES with SHIS (adjusted for geometric differences) show mean and standard deviation differences of less than 0.3 K at warmer brightness temperatures of 290–295 K. The TES/SHIS differences are less than 0.4 K at brightness temperatures of 265–270 K. There are larger TES/SHIS comparison differences for higher-frequency TES 1A1 filter, which has less upwelling radiance signal. The TES/AIRS comparisons show mean differences of less than 0.3 K at 290–295 K and less than 0.5 K at 265–270 K with standard deviation less than 0.6 K for the majority of the spectral regions and brightness temperature range. A procedure to warm up the optical bench for better alignment in December 2005 gave a fourfold increase in the signal-to-noise ratio at higher frequency ranges. Recent results from a long-term comparison of TES sea surface temperature (SST) observations with the Reynolds optimally interpolated (ROI) SST product demonstrates TES radiometric stability.

Citation: Shephard, M. W., et al. (2008), Tropospheric Emission Spectrometer nadir spectral radiance comparisons, *J. Geophys. Res.*, *113*, D15S05, doi:10.1029/2007JD008856.

1. Introduction

[2] The Tropospheric Emission Spectrometer (TES) is a Fourier Transform Spectrometer (FTS) flying on the NASA Aura platform [*Beer et al.*, 2001; *Beer*, 2006; *Schoeberl et al.*, 2006]. The fundamental measurements used in the TES retrievals are the upwelling infrared spectral radiances. Thus, accurate radiances are critical for both trace gas profile retrievals for air quality as well as radiative forcing for climate [*Gauss et al.*, 2003]. For example, any radiometric systematic errors (e.g., calibration) not addressed in the L1B radiances will propagate as errors in the retrieved parameters [*Bowman et al.*, 2006; *Worden et al.*, 2004]. The quality of the TES spectra has improved significantly since launch in July 2004; it is the purpose of this paper to provide a brief overview of the improvements and benchmark the current radiometric accuracy, principally through comparisons with instruments whose accuracy is well documented.

[3] TES has a number of observational modes (e.g., global survey, step-and-stare, transect). In global survey mode TES makes measurements along the satellite track for 16 orbits with a spacing of ~182 km; in step-and-stare mode nadir measurements are made every 40 km along the track for approximately 50° of latitude; in transect mode observations consist of series of 40 consecutive scans spaced 12 km apart. TES also has the capability to perform both nadir and limb viewing, but for the validations presented here we have focused on the nadir-viewing mode. TES nadir spectra have 0.06 cm^{-1} unapodized spectral resolution and have footprints of 8 × 5 km^2 resulting from the averages of 16 element detector arrays where each detector has a 0.5 × 5 km^2 nadir footprint. Figure 8 is an example of the TES nadir spectrum from 7 November 2004.

[1] Atmospheric and Environmental Research, Inc., Lexington, Massachusetts, USA.
[2] Jet Propulsion Laboratory, Pasadena, California, USA.
[3] Raytheon Technical Services Company, Pasadena, California, USA.
[4] University of Wisconsin-Madison, Madison, Wisconsin, USA.

0148-0227/08/2007JD008856$09.00

[4] TES L1B processing produces radiometrically and spectrally calibrated radiance spectra from L1A interferograms. Interferograms for calibration targets, i.e., the reference blackbody at 340 K and a view of cold space, are taken routinely so that nadir and limb earth views are bracketed in time with calibration measurements. For global survey observations, the time span between calibrations is 82 s and calibration scans are included in an optimal fit for time variability that also reduces their noise contribution through averaging. For special observations, the time spans are longer: 7.5 min for the transect mode and 17 min for the step-and-stare mode. Special observations use a linear-in-time interpolation of scan averages taken before and after the target observations. On the basis of studies of calibration stability, a linear interpolation over these bracketing timescales is sufficient to capture changes in the instrument-offset radiance.

[5] To calibrate an individual target scan with averaged, time interpolated cold space and blackbody spectra, the TES calibration algorithm follows the methods first proposed by *Revercomb et al.* [1988a] using complex calibration and target spectra to explicitly remove instrument phase errors. The TES L1B algorithm is described in detail in the Algorithm Theoretical Basis Document (ATBD) [*Worden and Bowman*, 1999] and results from the instrument-commissioning phase are given by *Worden et al.* [2006].

[6] In order to ascertain the quality of the TES radiances, comparisons were made between TES spectra and measurements from two other spectrometers, the Atmospheric Infrared Sounder (AIRS) on NASA's Aqua satellite [*Aumann et al.*, 2003] and the scanning high-resolution interferometer sounder (SHIS) flown on an aircraft. AIRS measures 2378 infrared radiances between 650 and 2665 cm^{-1} with a resolving power ($\lambda/\Delta\lambda$) of 1200 (e.g., 0.5 cm^{-1} at 600 cm^{-1}; 2.0 cm^{-1} at 2400 cm^{-1}). Brightness temperature comparisons of AIRS with SHIS show the AIRS radiometric accuracies to be ~0.2 K for most channels [*Tobin et al.*, 2006]. The SHIS design and calibration techniques have developed from experience with the HIS and from the ground based Atmospheric Emitted Radiance Interferometer (AERI) instruments developed for the DOE Atmospheric Radiation Measurement (ARM) program [*Revercomb et al.*, 1988a, 1988b, 1996]. For a description of the calibration approach and algorithms used for AERI, which are similar to SHIS, the reader is referred to *Knuteson et al.* [2004a, 2004b]. The SHIS has programmable cross-track scanning with ~2 km footprints when flying on an aircraft near the tropopause. The focus of the design of the SHIS has been on obtaining accurate calibration, and perturbation analysis of the radiometric calibration shows that the SHIS has absolute radiometric uncertainties of less than 0.15 K for scene brightness temperatures greater than 250 K.

[7] In section 2.1 comparisons between TES and AIRS are used to highlight the increased accuracy in the TES spectra due to changes in the TES L1B algorithm (version 1 (V001) to version 2 (V002)). In section 2.2 the improvement in the TES 1A1 band obtained through an optical bench warm up is discussed. In section 3, SHIS and AIRS radiance comparisons are used to validate the TES spectra. Section 4 presents an overview of TES sea surface temperature (SST) comparisons, which are used to show the long-term stability of the TES radiances.

2. TES Radiance Updates

2.1. TES L1B Algorithm Improvements

[8] Significant improvements to the L1B algorithms were made between data versions V001 and V002. The most significant updates are to the modeling the time dependence, and the improved sampling phase alignment. These changes included a more robust approach to the correction for the ambiguous linear sampling phase that can be different between scans and must be aligned before averaging and complex calibration can be performed. The complex calibration was computed using equation (1):

$$L_{\text{Target}} = \frac{C_{\text{Target}} - C_{\text{CS}}}{C_{\text{BB}} - C_{\text{CS}}} \varepsilon_{\text{BB}} B(T_{\text{BB}}), \tag{1}$$

where L_{Target} is the calibrated TES target radiance, C_{Target} is the complex target spectrum, C_{CS} is the complex cold space view spectrum, C_{BB} is the complex blackbody spectrum, ε_{BB} is the blackbody emissivity, and $B(T_{\text{BB}})$ is the Planck function for the blackbody at temperature T. Note that the contribution of the cold space blackbody (~3 K) is negligible. The optimal fit for time variability in global surveys calibration data was also included for V002 data. The most significant source of time variability over a global survey was the buildup of ice on the detector arrays (which is removed by decontamination cycles).

[9] Since the AIRS-Aqua is just 15 min ahead of TES-Aura on the "A-Train" orbit, TES comparisons with AIRS spectra were used as a metric for algorithm improvements. For the TES/AIRS comparison, 190 TES nadir targets from global survey 2147 (16 orbits) on 20 September 2004 that have a 0.5 K homogeneity in surface brightness temperatures across a detector array were identified. Fifty of these were also confirmed as homogenous for AIRS, as determined by the AIRS spatial uniformity tests discussed by *Aumann et al.* [2006]. These homogenous nadir targets are the cases used to evaluate the TES L1B algorithm improvements used for TES V002. Figure 1 shows the improvement in the TES/AIRS ratio in the V002 (Figure 1b) calibration as compared with V001 (Figure 1a). For the TES/AIRS comparison, the high-resolution TES spectrum was convolved directly with the lower-resolution AIRS SRF (spectral response function) provided for each AIRS channel. This direct application of the AIRS SRF to TES data, essentially assuming the TES spectrum is monochromatic, is accurate to within 0.002 K [*Sarkissian et al.*, 2005].

[10] Figures 2–4 show the frequency and time dependence of TES-AIRS comparisons for TES 2B1, 1B2, and 2A1 filters. These figures show results for single pixel comparisons. For each filter, the top panel shows the average over 50 nadir targets of the TES-AIRS brightness temperature difference as a function of frequency on the AIRS frequency grid. The bottom panels show averages over frequency as a function of target index or time, spanning about 26 h. These plots demonstrate how the different V002 improvements affect the TES frequency ranges. In the 2B1 filter, the most significant improvement is from modeling the time dependence, while in 1B2 and

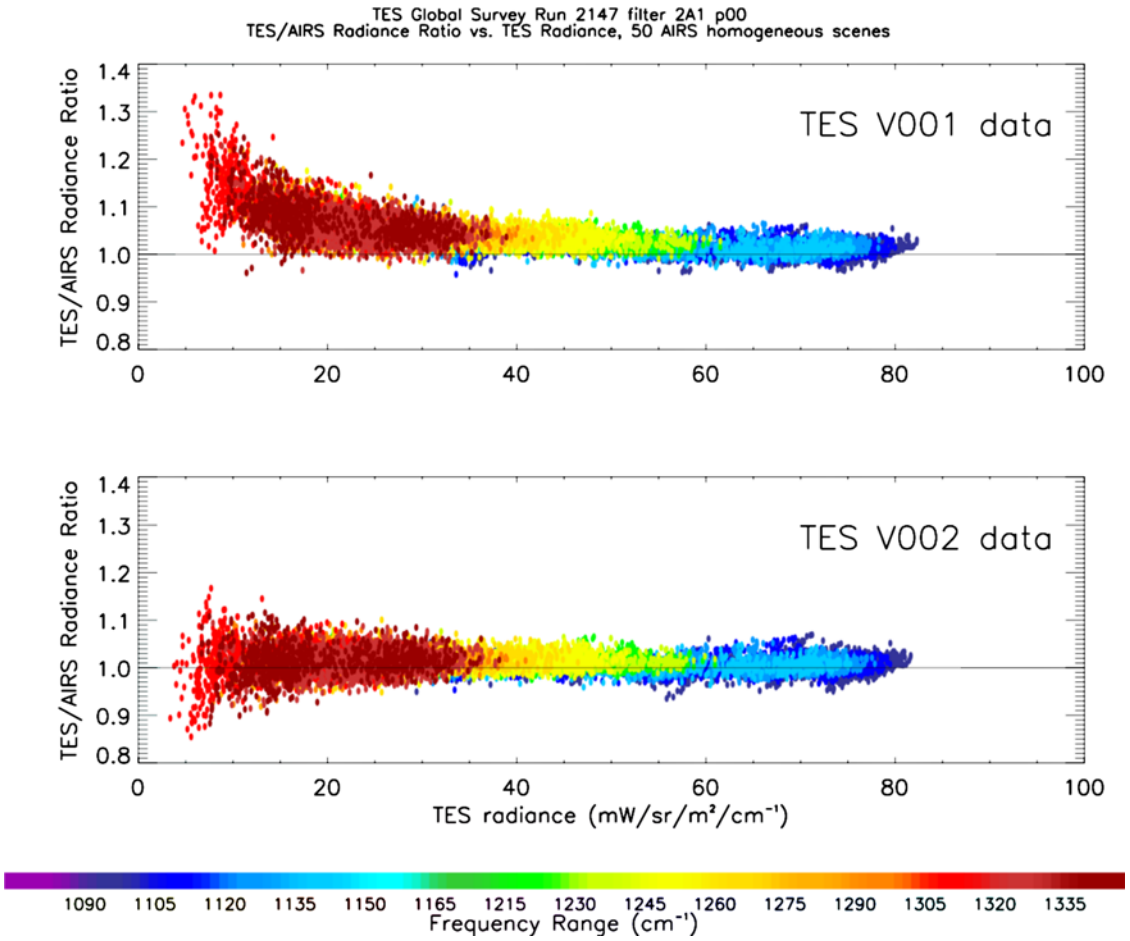

Figure 1. Plot of the radiance ratio (TES/AIRS) versus radiance and color coded for frequency ranges. (a) The spread in values over the homogenous cases for the baseline calibration in V001 and (b) for the improved V002 L1B calibration.

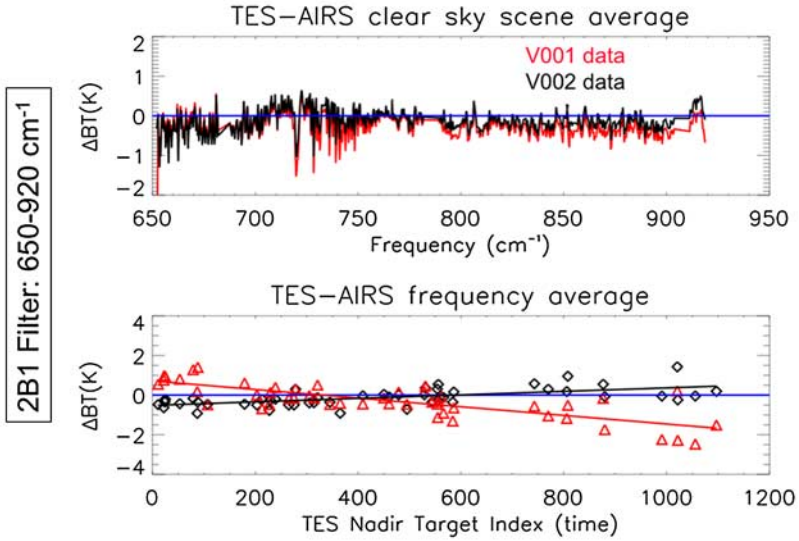

Figure 2. TES/AIRS radiance comparison in the 2B1 filter for 50 cases for the TES global survey 2147. (top) The brightness temperature difference as a function of frequency average over 50 cases. (bottom) The filter-averaged TES-AIRS brightness temperature difference for each case as a function of time along the TES global survey.

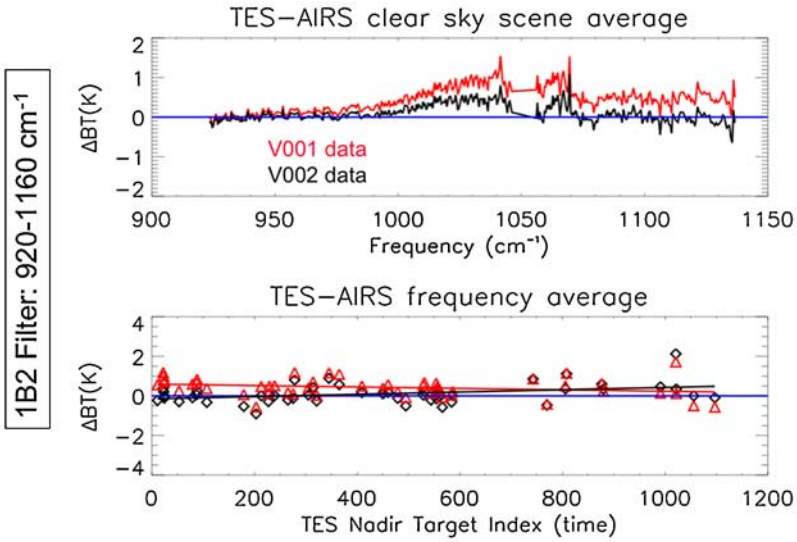

Figure 3. TES/AIRS radiance comparison in the 1B2 filter, using the same plotting convention as Figure 2.

2A1, the time dependence is nearly flat in both the baseline and prototype runs, as expected from the spectral dependence of ice absorption which has a broad peak centered around 830 cm^{-1}. For 1B2, and especially 2A1, we see large improvements due primarily to the improved sampling phase alignment. Table 1 contains V001 and V002 full-filter-averaged statistics for global survey 2147. Also included in the table are comparison results from global survey 2931 on 21 May 2005, which had 320 match-up target scenes. Note that the statistics in Table 1 are computed using TES 16 pixel scenes. These V002 L1B modifications have resulted in improved TES retrieval parameters as demonstrated, for example, in sea surface temperature retrievals, for V001 data versus V002 data (M. C. Lampel et al., Analysis of the Tropospheric Emission Spectrometer sea surface temperature for two years of observations, submitted to *Atmospheric Chemistry and Physics*, 2008, hereinafter referred to as Lampel et al., submitted manuscript, 2008), and in ozonesonde comparisons for V001 data [*Worden et al.*, 2007] versus V002 data [*Nassar et al.*, 2008]. Comparison results in the TES 1A1 filter are not shown here as these L1B improvements had much less impact on this band because of the very small contribution of the instrument background radiance at those frequencies. In addition, the overlap region between TES and AIRS in this filter is very small (2181–2251 cm^{-1}) and covers a spectral region not used for TES retrievals as it can contain a significant amount of unusable TES spectral "spikes" that are not easily identified at these low radiances. Analysis of the frequencies and amplitudes of the TES spectral spikes points directly to electromagnetic pickup of the analog-to-digital converter-sampling clock by the signal

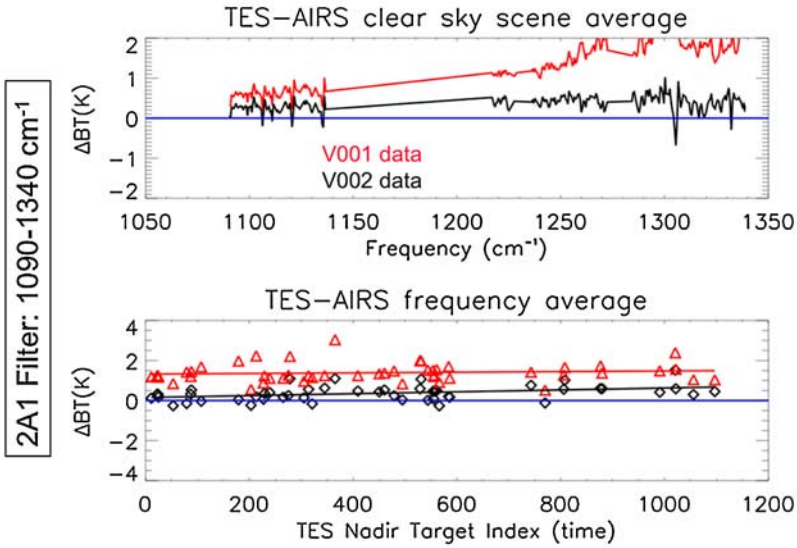

Figure 4. TES/AIRS radiance comparison in the 2A1 filter, using the same plotting convention as Figure 2.

Table 1. TES V001 and V002 Full Filter Radiance Comparisons[a]

		TES-AIRS			
		Run 2147 on 20 September 2004 (50 Target Scenes)		Run 2931 on 21 May 2005 (320 Target Scenes)	
TES Filter	Wave Number, cm^{-1}	Mean Δ BT, K	SD Δ BT, K	Mean Δ BT, K	SD Δ BT, K
2B1	650–920	−0.18 (−0.29)	0.46 (0.86)	−0.13 (−0.31)	0.42 (0.54)
1B2	920–1160	0.01 (−0.05)	0.48 (0.52)	−0.12 (−0.19)	0.38 (0.38)
2A1	1090–1340	0.34 (1.05)	0.36 (0.37)	0.35 (1.37)	0.32 (0.70)

[a]The evaluation statistics are averaged over the full filter, and the values in parentheses are from TES V001 release.

chains [*Beer et al.*, 2003]. The main improvement for radiances in the 1A1 filter was obtained from the on-orbit optical bench warm up.

2.2. TES Instrument Improvements: Optical Bench Warm Up

[11] The optical bench warm up was used to adjust and maintain the alignment of the instrument beam splitter, thus increasing the integrated spectral magnitude (ISM). The ISM is calculated as the integration of the raw spectrum for a given filter when the instrument views the onboard 340 K blackbody calibration source. The ISM calculation is performed routinely providing a sensitive measure of the trend in the mean signal levels at the detector. Figure 5 contains a plot of normalized Integrated Spectral Magnitude (ISM) that has been updated from the one presented by *Rinsland et al.* [2006] to cover the time period from launch until March 2007. From launch until the optical bench warm up, which took place between 29 November and 2 December 2005, there was a steady drop in ISM. The periodic jumps in the ISM corresponded to small increases in the optical bench temperature during routine decontamination for ice buildup, which was needed more frequently at the beginning of a mission. These increases confirmed the results from pre-launch calibration that the beam splitter alignment could be adjusted by changing the temperature of the optical bench. The optical bench warm up of 6 K resulted in an increase of a factor of 3.4 in the ISM. This improvement has a significant impact on retrievals using the 1A1 filter. For example, *Rinsland et al.* [2006] showed that the degrees of freedom for signal (DOFS), which is a measure of the number of independent pieces of information obtained in the retrieval [*Rodgers*, 2000], for CO increased by a factor of 2 (0.72 to 1.45 averaged for 30°S–30°N) after the optical bench warm up. Unfortunately there are no good comparison observations available for an external evaluation of the radiometric accuracy after the improvements because of the optical bench warm up. This is because AIRS does not have overlapping frequencies with the TES 1A1 filter in a region that is useful for comparisons and there are currently no available SHIS underpasses observations in cloud-free conditions after the optical bench warm up. However, in order to provide additional metrics on the impact of the optical bench warm up we compare noise equivalent spectral brightness temperature (NESBT) for TES filter 1A1 before and after the optical bench warm up. NESBT is computed from the noise equivalent spectral radiance (NESR) by adding it to the Planck function for the average spectral brightness temperature,

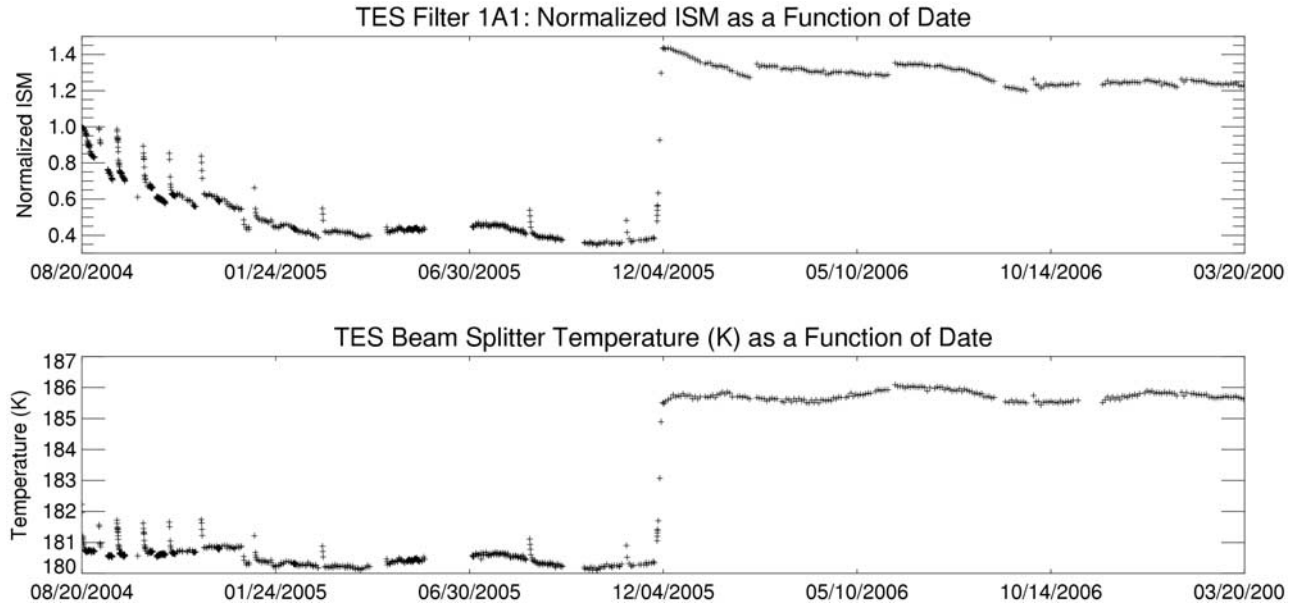

Figure 5. Time series of (top) normalized Integrated Spectral Magnitude (ISM) and (bottom) beam splitter temperature. The ISM is the area integration of the TES spectral radiance viewing the onboard hot calibration source, and they are normalized to 1.0 at the beginning of the time series.

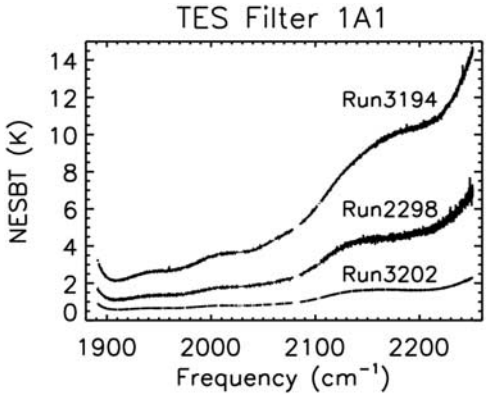

Figure 6. Plot of the TES 1A1 filter estimated noise equivalent source brightness temperature (NESBT) values as a function frequency. Run 3194 is a TES global survey on 27–28 November 2005 just before the optical bench warm up. Run 3202 is a TES global survey on 7–8 December 2005 just after the optical bench warm up. Also, plotted for reference is run 2298, which is the TES step-and-stare run used in the TES/SHIS comparisons. The criteria for the scans included in the plots are: latitudes between 20°S and 20°N, surface brightness temperatures between 290 and 295 K, and screened with the TES master quality flag. Each plot is the average NESBT for TES scans that are each 15 pixel detector averages.

converting from radiance to brightness temperature and subtracting off the average spectral brightness temperature. Figure 6 shows the NESBT plots for (1) run 3194, a TES global survey on 27–28 November 2005 just before the optical bench warm up; (2) run 3202, a TES global survey on 7–8 December 2005 just after the optical bench warm up; and (3) run 2298, which is the TES step-and-stare run used in the TES/SHIS comparisons and provided for reference. Comparing TES observations just before (run 3194) and after (run 3202) provides an estimate of the noise improvements in the TES 1A1 filter obtained from the optical bench warm up. Note that the NESBT values in Figure 6 are likely an overestimate of the noise due to unidentified spikes being included in the calculations, and therefore should mainly be interpreted in the context of showing the relative improvement of the optical bench warm up.

3. Radiance Validations

[12] TES nadir spectral radiances have been validated against both SHIS and AIRS. Here we show examples of the radiance comparisons used to validate the TES observed radiances.

3.1. TES/SHIS Radiance Comparison

[13] During the Aura Validation Experiment (AVE) there were several SHIS underflights of TES. We studied two cloud-free scans on 7 November 2004 where SHIS flew under the TES overpass at an altitude of 18 km over the Gulf of Mexico. The absence of clouds is determined by the zero cloud fraction retrieved by the Moderate Resolution Imaging Spectroradiometer (MODIS) and by the small variability in the 1103–1105 cm^{-1} window brightness temperatures demonstrated in the TES and SHIS scans in Figure 7. The brightness temperatures plotted here have not been corrected for any geometric difference between the two sensors, therefore, given that TES is flying at a much higher altitude the TES brightness temperatures in the window region are expected to be cooler. An average TES spectrum for each scan was obtained by averaging the sixteen TES pixels; a corresponding SHIS spectrum was constructed by averaging the nine closest SHIS scans to the center of the TES scan. The SHIS footprints in Figure 7 show the SHIS scans used in the comparisons. Unfortunately, there were no coincident AIRS observations available at this time.

[14] In order to compare the spectra from the different instruments line-by-line radiative transfer model (LBLRTM) [*Clough et al.*, 2005] forward model calculations were

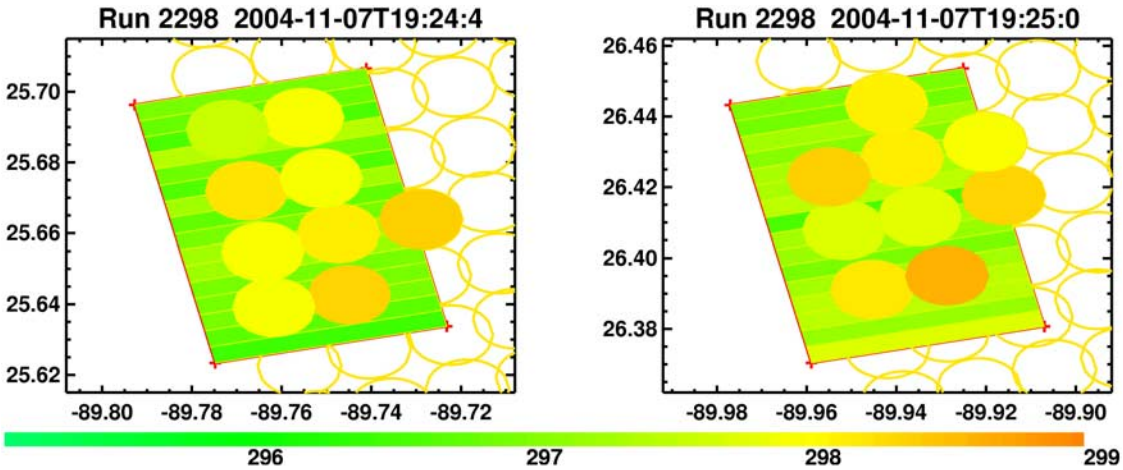

Figure 7. Brightness temperature in the 1103–1105 cm^{-1} microwindow for TES nadir scans (run 2298, sequence 3, scans 8 and 10), each consisting of 16 0.5 × 5 km^2 rectangular pixels and 9 SHIS scans for the corresponding underflight; SHIS scans are ~2 km circles.

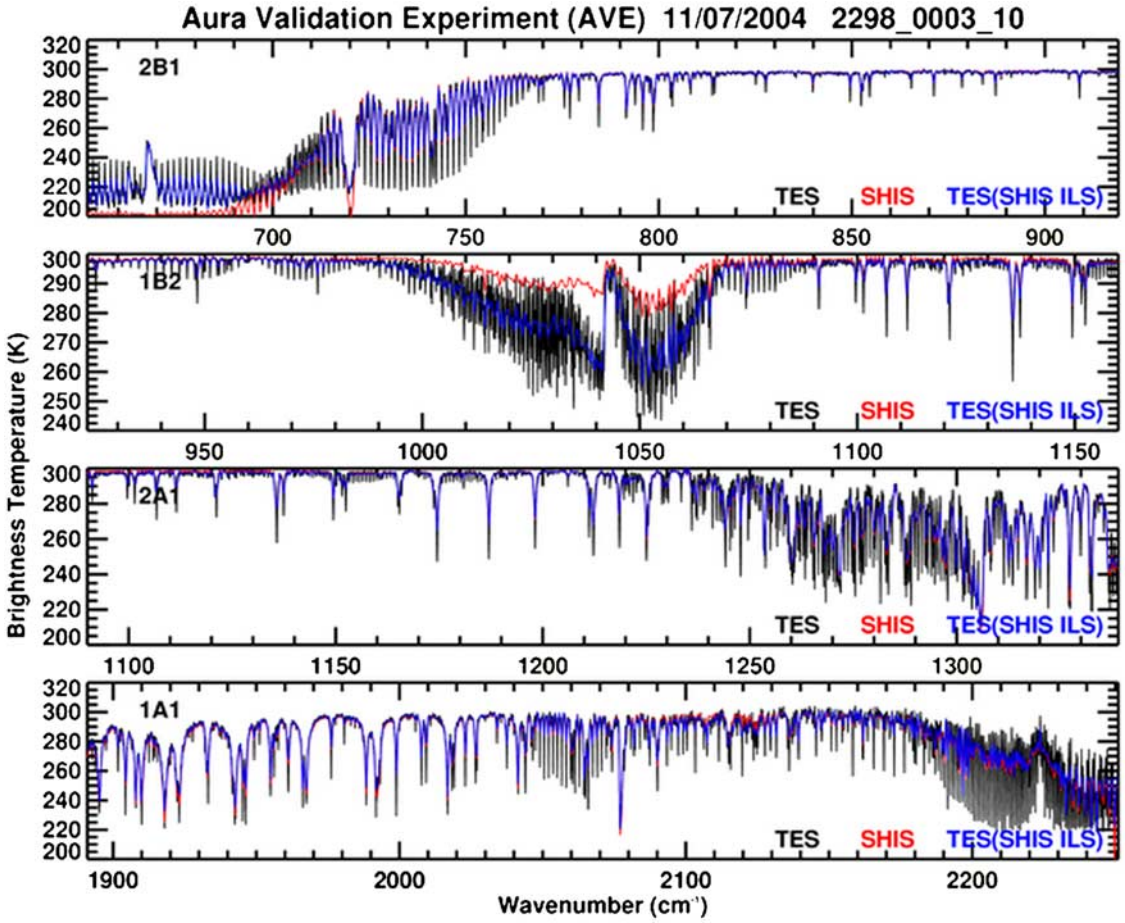

Figure 8. Same example TES nadir spectrum from 7 November 2004 for filters 2B1, 1B2, 2A1, and 1A1, but with the SHIS (red lines) and the TES spectral convolved with the SHIS ILS (blue lines) overplotted.

utilized to account for the differences between altitude and viewing angles (see equation (2))

$$[\text{TES} * \text{SHIS ILS} - ((\text{LBLRTM} * \text{TES ILS}) * \text{SHIS ILS})] - [\text{SHIS} - (\text{LBLRTM} * \text{SHIS ILS})], \quad (2)$$

where * is the convolution operator. This follows the approach used to provide accurate and detailed assessment of the AIRS spectral radiance observations [*Tobin et al.*, 2006]. Implicit in this procedure is the assumption that the modeled atmosphere between the aircraft altitude and the satellite is representative of the true atmosphere. When the atmosphere specified above the nadir SHIS observation (18 km) does not represent the true atmospheric state there will be additional residuals in the spectral regions where there is emission above the aircraft.

[15] TES and SHIS have spectral resolutions of 0.06 and 0.48 cm^{-1}, respectively. In order to put the two sensors on the same resolution for comparison purposes, TES was convolved with SHIS instrument line shape (ILS). Figure 8 shows a TES, SHIS, and TES spectra convolved with the SHIS ILS (TES*SHIS ILS) for TES run 2298, sequence 3, scan 10 on 7 November 2004. Noticeable differences between TES and SHIS are evident in the spectral regions where there is significant emission above the aircraft (e.g., CO_2 and O_3 spectral regions). An example of the TES-SHIS spectral comparisons, as defined by equation (2), for the 2B1, 1B2, 2A1, and 1A1 TES filters for scan 10 are shown in Figure 9. Note that more detailed TES spike remove was performed on the TES observations for these comparisons because the full filter forward model calculations used to account for the geometric differences in equation (2) were also used to further identify TES spikes; any 4σ (TES-LBLRTM) spectral points were removed from the statistics. Over most of the TES spectral regions there is good agreement with SHIS. The largest residuals are in the regions with significant emission above the aircraft (e.g., CO_2 ν_2 ($\sim$650–700 cm^{-1} in the 2B1), O_3 (1020–1060 cm^{-1} in the 1B2), CH_4 ν_4 (Q branch at 1306 cm^{-1} in the 2A1), and the start of the CO_2 ν_3 (the 2180–2251 cm^{-1} in the 1A1)). As stated earlier, incorrect specification of the atmosphere above the aircraft will result in differences beyond the differences in the instrument radiances themselves. In addition, incorrect specification of the atmosphere in a region in which one sensor is more sensitive to than the other will also generate differences that are not due to radiances themselves. For example, a sensor flying on an aircraft will in general be more sensitive to the atmosphere

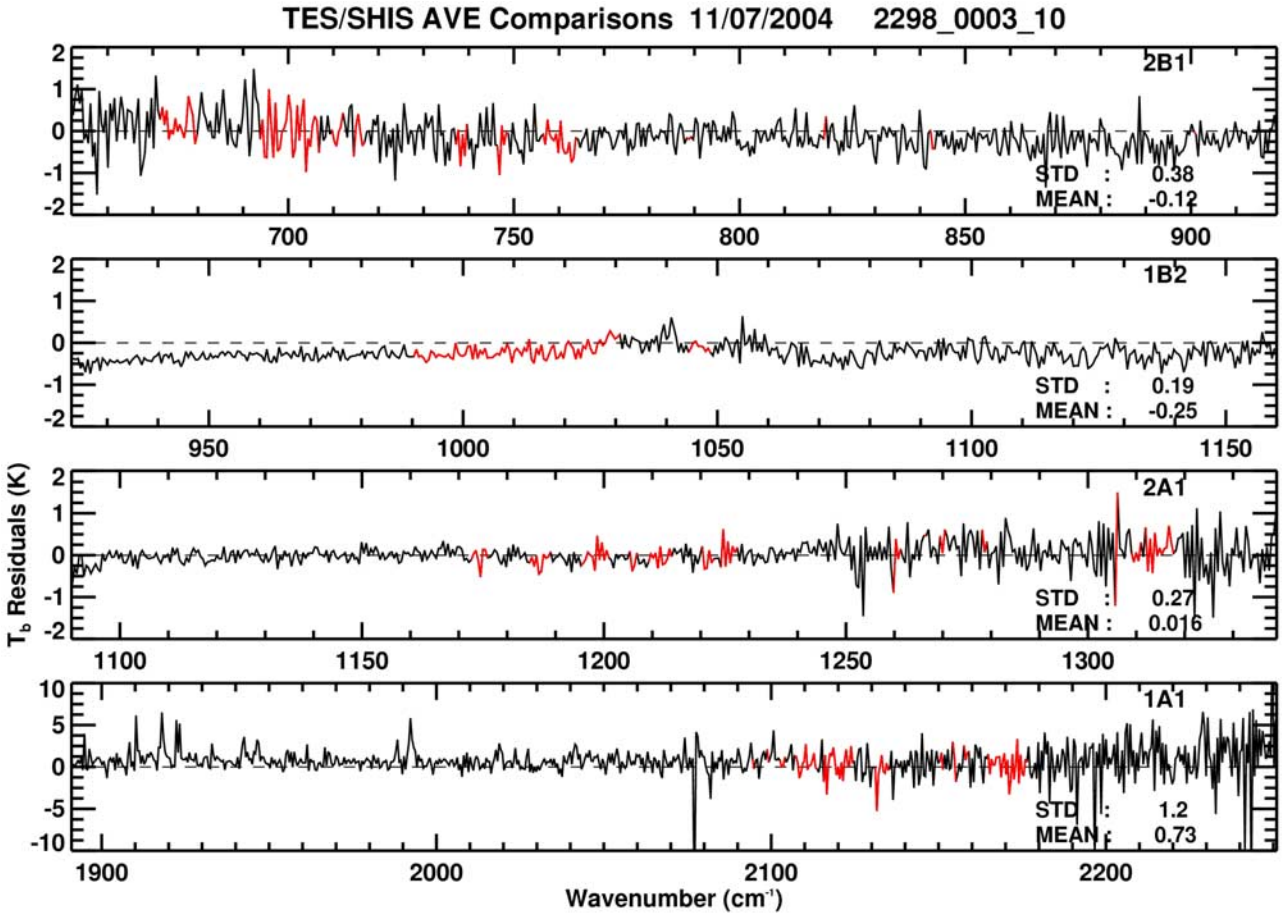

Figure 9. Difference between TES and SHIS brightness temperature residuals for run 2298, sequence 3, scan 10 at the SHIS resolution for filters 2B1, 1B2, 2A1, and 1A1. TES V002 L1B radiances were used in this comparison. The red lines are the TES microwindows presently used in TES retrievals.

just below the aircraft than an instrument observing from space (e.g., temperature and ozone). Since there were no coincident and collocated sonde profiles available to specify the atmosphere state, the TES retrieved profile was used in the calculations. The TES a priori profile calculated from the GEOS global transport model maintained at NASA's Global Modeling and Assimilation Office (GMAO) [*Bloom et al.*, 2005] was tried (not shown), however it did not characterize the atmosphere as well as the TES retrieved profile.

[16] Additional insight from these comparisons is obtained from scatterplots of the combined brightness temperature differences from both scans 8 and 10 as a function of brightness temperature (Figure 10). There are small but systematic differences between the TES and SHIS at warmer temperatures near the surface (285–300 K); filter 2B1 has a difference of −0.2 K, 1B2 of −0.28 K, 2A1 differences are very close to zero, and the 1A1 band has a systematic difference of 0.5K. The 2B1 differences become slightly positive at wave numbers below 700 cm^{-1}, where emission is mainly from the tropopause region. The 1B2 differences show a distinctive increase with decreasing temperature and wave number, as the emission moves into the O_3 band. Detailed TES-SHIS comparison statistics for 5 K temperature bins at 265–270 K and 290–295 K are in Table 2. It should be pointed out that the signal in the 1A1 region is low because of the cold temperatures and drop off in radiance of the blackbody plank function at these wave numbers and temperatures. Therefore, differences due to noise or spikes in the TES radiances will result in large brightness temperature differences in the 1A1 filter, especially at the high frequencies and cooler temperatures.

3.2. TES/AIRS Radiance Comparison

[17] A different perspective on the TES-AIRS differences can be obtained from the same data set presented in section 2.1 by plotting the TES-AIRS residuals as a function of the TES brightness temperature and frequency (Figure 11). For this analysis only clear-sky scenes over ocean were used; a scene was determined to be clear using brightness temperature interpixel variability (16 pixel standard deviation <0.25 K), absolute brightness temperature (greater than 273 K), and the lapse rate (greater than 3°C/km). Each of the bands reveals an interesting aspect of the TES-AIRS differences. The 2B1 differences are close to zero across most of the band (from the surface to the tropopause) and become negative at cooler temperatures in the part of the CO_2 ν_2 (650–680 cm^{-1}) band where the emission is mainly from the tropopause and above. The 1B2 differences are

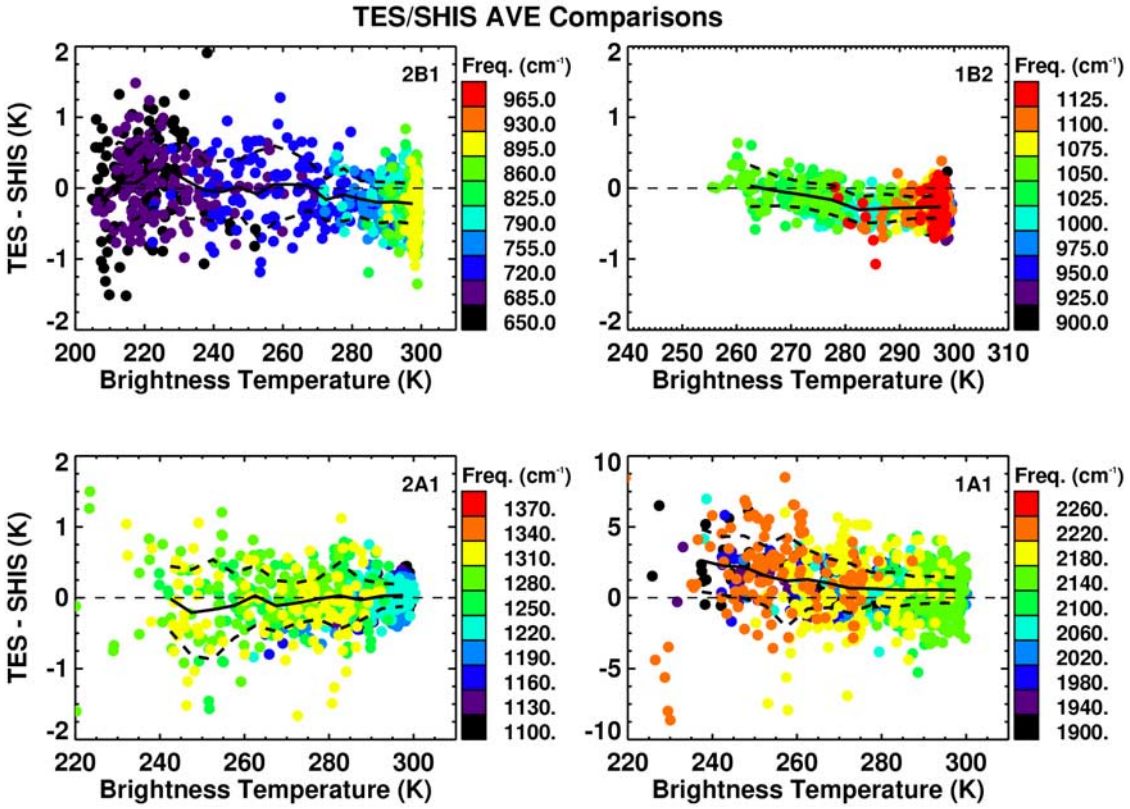

Figure 10. Scatterplots of TES-SHIS brightness temperature differences as a function of brightness temperature and color coded in frequency bins for run 2298, sequence 3, scans 8 and 10. The bold dashed lines are the 1σ standard deviation, and the solid line is the mean. TES V002 L1B radiances are used in the comparison.

also zero near the surface, but become positive (0.3–0.4 K) at the cooler temperatures associated with the ozone stratospheric emission (1020–1040 cm^{-1}). Finally, the residuals in the 2A1 band are approximately constant over the entire band with average difference values between 0.3 and 0.5 K, even at the surface, where the residuals in 2B1 and 1B2 are zero. Some of the TES-AIRS comparison differences maybe attributed to the fact that the two observations may not be observing exactly the same atmosphere (e.g., water vapor, unscreened clouds, etc.) as they are not simultaneous measurements (15 min apart) and have different fields of view. Detailed statistics for 5 K temperature bins at 265–270 K and 290–295 K can be found in Table 2. The TES-AIRS standard deviations are larger than the TES-SHIS reported in Table 2. This might be due to the fact that TES-AIRS comparison covers a wider range of atmospheric states than the TES-SHIS comparison, and/or that SHIS is a better-calibrated instrument, especially when you consider that nine SHIS footprints are averaged together in one TES scene.

4. TES Radiance Validation From SST Measurements

[18] In addition to direct AIRS and SHIS radiance comparisons, TES radiances can be indirectly validated through

Table 2. TES V002 Clear-Sky Radiance Comparisons With AIRS and SHIS[a]

TES Filter	Wave Number, cm^{-1}	Brightness Temperature, K	TES-AIRS Run 2147 on 20 September 2004 (43 Clear-Sky Scenes) Mean Δ BT, K	TES-AIRS Run 2147 on 20 September 2004 (43 Clear-Sky Scenes) STD Δ BT, K	TES-SHIS Runs 2298 0003 08 and 2298 0003 10 on 7 November 2004 Mean Δ BT, K	TES-SHIS Runs 2298 0003 08 and 2298 0003 10 on 7 November 2004 STD Δ BT, K
2B1	650–920	290–295	−0.07	0.61	−0.19	0.27
		265–270	0.08	0.56	0.03	0.35
1B2	920–1160	290–295	−0.02	0.50	−0.28	0.15
		265–270	0.44	0.45	−0.04	0.21
2A1	1090–1340	290–295	0.26	0.59	0.02	0.18
		265–270	0.49	0.41	−0.11	0.36
1A1	1891–2251	290–295			0.56	0.94
		265–270			1.03	1.73

[a]The statistics are for 1 σ.

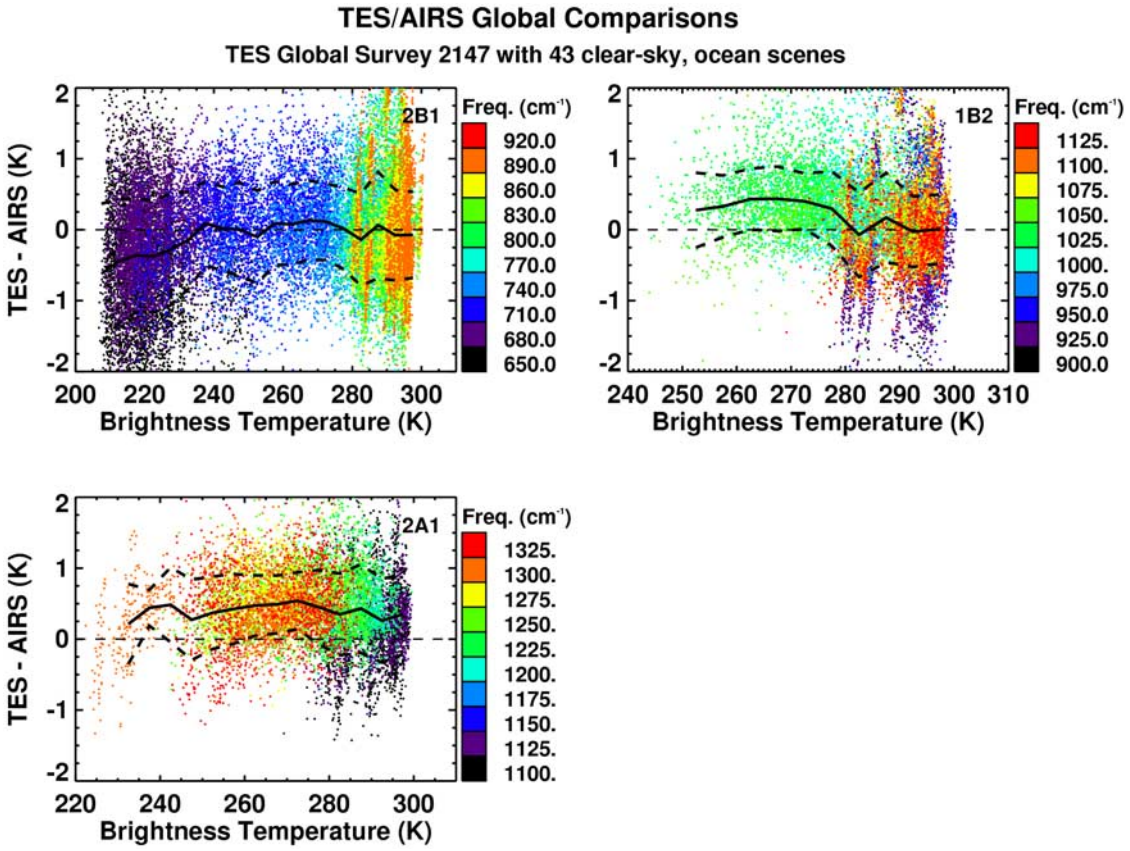

Figure 11. Scatterplots of TES-AIRS brightness temperature differences as a function of brightness temperature and color coded in frequency bins for 43 global clear-sky cases over the ocean. The bold dashed lines are the 1σ standard deviation, and the solid line is the mean.

comparisons of retrieved sea surface temperature (SST) [e.g., *Hagan and Minnett*, 2003; *Aumann et al.*, 2006]. These SST comparisons by Lampel et al. (submitted manuscript, 2008) for clear-sky radiances (retrieved effective cloud optical depth $\leq$0.05) over 2 years, demonstrates the long-term stability of TES measurements. It is important to note that the DOFS for the SST retrievals are generally close to 1 for these clear-sky cases and therefore the TES SSTs are not biased by the a priori. Lampel et al. (submitted manuscript, 2008) shows the time series of the SST bias with respect to Reynolds optimally interpolated (ROI) monthly average SST from November 2004 through November 2006 for nighttime and daytime. The ROI data set has the advantage that it is insensitive to clouds. In addition, the ROI is a bulk SST measurement allowing for a skin-bulk SST comparison, which can be used to determine the sensitivity of the TES SST retrievals. The average nighttime bias over this period is -0.17 K and the daytime average bias is 0.04 K, which is the expected difference between skin (TES) and bulk (ROI) temperature measurements. This ability to measure a skin-bulk temperature difference that is consistent with the expected physical skin-bulk nighttime bias of $\sim$0.2 K, clearly shows that TES has a sensitivity at the 0.1 K level. RMS differences of $\sim$0.5 K are consistent with the other comparison results shown in this paper. These results demonstrate that TES calibration has been very stable over the 2 year period. It is also important to note that D. Tremblay et al. (unpublished data, 2008) provides further evidence that the a priori does not bias the SST retrievals under clear-sky conditions. They provide a case study in which the a priori surface temperatures over Lake Tahoe were 17 K higher than the retrieved values (because of the fact that land surface temperature were used instead of water surface temperatures), however, the retrieved surface temperatures still compare quite well with the in situ measurements with a bias of -0.11 K and standard deviation of 0.30 K.

5. Discussion and Concluding Remarks

[19] Radiance comparison case studies of TES with SHIS and AIRS are utilized to estimate the in-orbit radiometric calibration of TES. The mean and standard deviation of TES differences with both AIRS and SHIS are presented. TES/SHIS comparisons show a mean difference of less than

Table 3. Spectral Ranges for TES Filters Commonly Used in the Nadir

Filter Identification	L1B Minimum	L1B Maximum	Suggested Minimum for L2	Suggested Maximum for L2
2B1	652	919	660	910
1B2	923	1160	950	1130
2A1	1090	1339	1120	1320

0.3 K with a standard deviation of 0.3 K for brightness temperatures at 290–295 K, except for the 1A1 filter where the reduced signal increases the brightness temperature differences. Note that TES comparisons with both AIRS and SHIS at these warmer brightness temperatures (near the surface) show that the 2B1 and 1B2 filters agree with each other, but the 2A1 filter is 0.2–0.3 K warmer. If not taken into consideration this systematic error will impact retrievals that use multiple filters (e.g., TES temperature and cloud retrievals). The TES/SHIS comparison results for cooler brightness temperatures show mean differences less than 0.2 K with standard deviation less than 0.4 K at 265–270 K. Since some of these comparisons at the cooler brightness temperatures are from spectral regions where there is significant contribution from the atmospheric emission, it is likely that the differences are greater than the differences in the instrument radiances themselves because of errors in the input profiles used to account for the atmosphere between the aircraft. The TES/AIRS comparison show a mean difference of less than 0.3 K with a standard deviation of 0.6 K at brightness temperatures 290–295 K. Comparisons at cooler brightness temperatures 265–270 K show TES/AIRS mean and standard deviation differences of 0.5 K and 0.6 K, respectively.

[20] It must be noted that TES calibration errors increase significantly within about 10 cm^{-1} of the half-power point frequencies of the optical filters. A study by H. Revercomb et al. (unpublished data, 2006) suggests the errors are likely due to a phase modulation resulting from interferometer velocity variations. These errors are mitigated in the L2 retrieval by the selection of frequency ranges that do not include the filter edges. Table 3 lists the useable spectral ranges that were determined on the basis of the radiance comparisons.

[21] Even though great efforts have been made to obtain coincident and colocated radiance observations under conditions in which the true state of the atmosphere is known, this is a challenging task. In addition, TES radiance validation is ongoing since instrument properties can change over the mission lifetime. Future radiance comparisons (e.g., with SHIS) under cloud-free conditions, over water (where the infrared emissivity is well known), and where the atmosphere has been well characterized (e.g., radiosondes, ozonesondes, etc.) would be extremely useful for this validation effort. In addition, TES/AIRS radiance comparison results can be further refined in the future by including more comparisons. This article has focused on nadir observations that have a greater potential for coincident measurements. Validation of TES limb radiances will rely heavily on model comparisons and will be addressed in a future publication.

[22] **Acknowledgments.** We would like to thank Eli Mlawer and Ted Kennelly at AER for their helpful discussions. We would also like to thank George Aumann (JPL) for supplying us with AIRS match-up data, the reviewers, and the associate editor for their very constructive comments. This work was supported by the Jet Propulsion Laboratory, California Institute of Technology, under a contract with the National Aeronautics and Space Administration. Part of the TES Aura data used in this research was obtained from the NASA Langley Research Center Atmospheric Sciences Data Center. The AQUA MODIS cloud data was obtained from NASA's L1 and Atmospheric Archive and Distribution System (LAADS WEB) website (http://ladsweb.nascom.nasa.gov/).

References

Aumann, H. H., et al. (2003), AIRS/AMSU/HSB on the Aqua mission: Design, science objectives, data products, and processing systems, *IEEE Trans. Geosci. Remote Sens.*, *41*, 253–264, doi:10.1109/TGRS.2002.808356.

Aumann, H. H., S. Broberg, D. Elliott, S. Gaiser, and D. Gregorich (2006), Three years of AIRS radiometric calibration validation using sea surface temperatures, *J. Geophys. Res.*, *111*, D16S90, doi:10.1029/2005JD006822.

Beer, R. (2006), TES on the Aura mission: Scientific objectives, measurements and analysis overview, *IEEE Trans. Geosci. Remote Sens.*, *44*(5), 1102–1105, doi:10.1109/TGRS.2005.863716.

Beer, R., T. A. Glavich, and D. M. Rider (2001), Tropospheric Emission Spectrometer for the Earth Observing System's Aura satellite, *Appl. Opt.*, *40*, 2356–2367, doi:10.1364/AO.40.002356.

Beer, R., et al. (2003), Tropospheric Emission Spectrometer instrument calibration report, vols. 1 and 2, *JPL D-26533*, Jet Propul. Lab., Pasadena, Calif. (Available at http://tes.jpl.nasa.gov)

Bloom, S., et al. (2005), Documentation and validation of the Goddard Earth Observing System (GEOS) data assimilation system—Version 4, *Tech. Rep. on Global Model. and Data Assim. 104606*, vol. 26, Goddard Space Flight Cent., Greenbelt, Md. (Available at http://gmao.gsfc.nasa.gov/pubs/)

Bowman, K. W., et al. (2006), Tropospheric emission spectrometer: Retrieval method and error analysis, *IEEE Trans. Geosci. Remote Sens.*, *44*(5), 1297–1307, doi:10.1109/TGRS.2006.871234.

Clough, S. A., M. W. Shephard, E. J. Mlawer, J. S. Delamere, M. J. Iacono, K. Cady-Pereira, S. Boukabara, and P.D. Brown (2005), Atmospheric radiative transfer modeling: A summary of the AER codes, *J. Quant. Spectrosc. Radiat. Transfer*, *91*, 233–244, doi:10.1016/j.jqsrt.2004.05.058.

Gauss, M., et al. (2003), Radiative forcing in the 21st century due to ozone changes in the troposphere and the lower stratosphere, *J. Geophys. Res.*, *108*(D9), 4292, doi:10.1029/2002JD002624.

Hagan, D., and P. Minnett (2003), AIRS radiance validation over ocean from sea surface temperature measurements, *IEEE Trans. Geosci. Remote Sens.*, *41*, 432–441, doi:10.1109/TGRS.2002.808316.

Knuteson, R. O., et al. (2004a), Atmospheric Emitted Radiance Interferometer. part I: Instrument design, *J. Atmos. Oceanic Technol.*, *21*, 1763–1776, doi:10.1175/JTECH-1662.1.

Knuteson, R. O., et al. (2004b), Atmospheric Emitted Radiance Interferometer. part II: Instrument performance, *J. Atmos. Oceanic Technol.*, *21*, 1777–1789, doi:10.1175/JTECH-1663.1.

Nassar, R., et al. (2008), Validation of Tropospheric Emission Spectrometer (TES) nadir ozone profiles using ozonesonde measurements, *J. Geophys. Res.*, doi:10.1029/2007JD008819, in press.

Revercomb, H., D. L. Buijs, H. B. Howell, W. Smith, and L. Sromovsky (1988a), Radiometric calibration of IR Fourier transform spectrometers: Solution to a problem with the high-resolution interferometer sounder, *Appl. Opt.*, *27*, 3210–3218.

Revercomb, H. E., D. D. LaPorte, W. L. Smith, H. Buijs, D. G. Murcray, F. J. Murcray, and L. A. Sromovsky (1988b), High-altitude aircraft measurements of upwelling IR radiance: Prelude to FTIR from geosynchronous satellite, *Mikrochim. Acta*, *95*, 439–444, doi:10.1007/BF01349804.

Revercomb, H. E., et al. (1996), Airborne and ground-based Fourier transform spectrometers for meteorology: HIS, AERI and the new AERI-UAV, paper presented at Optical Instruments for Weather Forecasting Meeting, Soc. for Opt. Eng., Bellingham, Wash.

Rinsland, C. P., et al. (2006), Nadir measurements of carbon monoxide (CO) distributions by the Tropospheric Emission Spectrometer instrument onboard the Aura Spacecraft: Overview of analysis approach and examples of initial results, *Geophys. Res. Lett.*, *33*, L22806, doi:10.1029/2006GL027000.

Rodgers, C. D. (2000), *Inverse Methods for Atmospheric Sounding: Theory and Practice*, World Sci., Hackensack, N. J.

Sarkissian, E., et al. (2005), TES Radiometric Assessment, *Eos Trans. AGU*, *86*(52), Fall Meet. Suppl., Abstract A41A-0007.

Schoeberl, M. R., et al. (2006), Overview of the EOS Aura mission, *IEEE Trans. Geosci. Remote Sens.*, *44*(5), 1066–1074, doi:10.1109/TGRS.2005.861950.

Tobin, D.C., et al. (2006), Radiometric and spectral validation of Atmospheric Infrared Sounder observations with the aircraft-based Scanning High-Resolution Interferometer Sounder, *J. Geophys. Res.*, *111*, D09S02, doi:10.1029/2005JD006094.

Worden, H. M., and K. W. Bowman (1999), Tropospheric Emission Spectrometer (TES) level 1B algorithm theoretical basis document (ATBD), V. 1.1, *JPL D-16479*, Jet Propul. Lab., Pasadena, Calif. (Available at http://tes.jpl.nasa.gov/docsLinks/documents.cfm)

Worden, H., R. Beer, K. Bowman, B. Fisher, M. Luo, D. Rider, E. Sarkissian, D. Tremblay, and J. Zong (2006), TES level1 algorithms: Interferogram processing, geolocation, radiometric and spectral calibration, *IEEE Trans. Geosci. Remote Sens.*, *44*(5), 1288–1296, doi:10.1109/TGRS.2005.863717.

Worden, H. M., et al. (2007), Comparisons of Tropospheric Emission Spectrometer (TES) ozone profiles to ozonesondes: Methods and initial results, *J. Geophys. Res.*, *112*, D03309, doi:10.1029/2006JD007258.

Worden, J., S. S. Kulawik, M. W. Shephard, S. A. Clough, H. M. Worden, K. Bowman, and A. Goldman (2004), Predicted errors of Tropospheric Emission Spectrometer nadir retrievals from spectral window selection, *J. Geophys. Res.*, *109*, D09308, doi:10.1029/2004JD004522.

R. Beer, K. W. Bowman, B. M. Fisher, M. Gunson, M. Luo, G. B. Osterman, D. M. Rider, E. Sarkissian, and H. M. Worden, Jet Propulsion Laboratory, 4800 Oak Grove Drive, Pasadena, CA 91109, USA.

K. E. Cady-Pereira, S. A. Clough, and M. W. Shephard, Atmospheric and Environmental Research, Inc., 131 Hartwell Avenue, Lexington, MA 02421-3126, USA. (mshephar@aer.com)

M. Lampel and D. Tremblay, Raytheon Technical Services Company, 299 N Euclid Avenue, Suite 500, Pasadena, CA 91101, USA.

H. E. Revercomb and D. C. Tobin, University of Wisconsin-Madison, 1011 Atmospheric Oceanic and Space Sciences Building, Madison, WI 53706, USA.